Brazilian Journal
of Chemical
Engineering

ISSN 0104-6632
Printed in Brazil
www.abeq.org.br/bjche

Vol. 24, No. 02, pp. 233 - 248, April - June, 2007

A NUMERICAL INVESTIGATION OF THE AERODYNAMICS OF A FURNACE WITH A MOVABLE BLOCK BURNER

T. J. Fudihara[1], L. Goldstein Jr.[1] and M. Mori[2*]

[1]Thermal and Fluids Engineering Department, School of Mechanical Engineering,
State University of Campinas, P.O. Box 6122, 13.083-970, Campinas - SP, Brazil.
E-mail: leonardo@fem.unicamp.br
[2]Chemical Processes Department, School of Chemical Engineering,
State University of Campinas, P.O. Box 6066, 13.081-970, Campinas - SP, Brazil.
E-mail: mori@feq.unicamp.br

(Received: October 20, 2006 ; Accepted: April 23, 2007)

Abstract - In this work the air flow in a furnace was computationally investigated. The furnace, for which experimental test data are available, is composed of a movable block burner connected to a cylindrical combustion chamber by a conical quarl. The apertures between the movable and the fixed blocks of the burner determine the ratio of the tangential to the radial air streams supplied to the furnace. Three different positions of the movable blocks were studied at this time. A three-dimensional investigation was performed by means of the finite volume method. The numerical grid was developed by the multiblock technique. The turbulence phenomenon was addressed by the RNG k-ε model. Profiles of the axial, tangential and radial velocities in the combustion chamber were outlined. The map of the predicted axial velocity in the combustion chamber was compared with a map of the experimental axial velocity. The internal space of the furnace was found to be partially filled with a reverse flow that extended around the longitudinal axis. A swirl number profile along the furnace length is presented and shows an unexpected increase in the swirl in the combustion chamber.
Keywords: Furnace Aerodynamics; Swirling Flow; CFD Modeling.

INTRODUCTION

A gas furnace is an enclosure in which heat is generated by the combustion of a fuel gas. A basic furnace is composed of a burner connected to a combustion chamber by a quarl.

Gas burners are an apparatus through which a combustible gas, whether premixed or not with air, is released to burn, forming a steady flame, and which have a geometry such that an appropriate heat release pattern is attained in the combustion chamber. They control the various physical and chemical processes that develop in a combustion chamber, such as the mixing of reagents and the generation of combustion products, by directing the flux and the trajectory of the reactants, which emerge in the combustion chamber as a high velocity jet.

There is a class of burners that basically induces the jet to a swirling flow by channeling the flow or employing rotating mechanical devices (Beér and Chigier, 1974).

In an isothermal or inert jet, as in the present case, swirl acts to enhance the rate of jet growth and entrainment and reduces the mean flow velocity. In a reacting system, besides the previous effect, swirl induces a recirculation zone that primarily helps to obtain flame stabilization by providing the aerodynamic blockage and the reduced velocities necessary to stabilize a flame. The reverse flow zone cyclically transports hot combustion products from

*To whom correspondence should be addressed

downstream regions into the flame region. Despite the dilution effect, the high temperature products work as an energy source for preheating and ignition assistance (Beér and Chigier, 1974).

The quarl attenuates flow expansion when the fluid leaves the burner and enters the combustion chamber and helps the jet to follow the slope of the combustion chamber wall, increasing the adverse pressure gradient along the centerline, which is advantageous in decelerating the flow.

The existence of turbulent swirling flow in a combustion chamber of a furnace is central to control of the combustion process. This flow is strongly dependent on the geometry and boundary conditions.

In simulating the flow performance via numerical computations, it is important to specify properly the inlet boundary conditions. Yet past numerical simulation studies of the combustion chamber significantly simplified inlet conditions because of their complexities, especially inlet radial velocity, which was taken to be zero. In almost all of the past numerical simulations, fuel or fuel-air was injected into the combustion chamber in a central jet with the swirling air introduced around it. Axial and tangential velocity profiles, if not measured, were often assumed to be simple flat, linear or parabolic profiles. Such approaches eliminate the need to model the inlet systems directly, but produce unreliable predictions (Sloan et al., 1986; Dong and Lilley, 1994)

The first studies on combustion in swirling flow were reviewed by Syred and Beér, 1974; Lilley, 1977; Gupta et al., 1984 and others. More recently, papers by Vanoverberghe et al., 2003 and Mondal et al., 2004 included an extensive reference list with the most recent works on the subject.

In 1994, Dong and Lilley studied isothermal flows in a combustion chamber and tested the influence of the assumed axial and tangential inlet velocity profiles at the boundaries. They utilized a two-dimensional axis-symmetrical model and the k-ε turbulence model with the inlet radial velocity set to zero. Experimentally measured inlet velocity profiles were also tested, this time with a nonzero radial component. They concluded that the experimental inlet profiles should be preferred for a more realistic simulation of the flow field in the combustion chamber. In 1997, however, Xia et al., 1997, pondered that it looked like only the inlet swirl number was preserved in Dong and Lilley's simulation and not, simultaneously, the total mass flow rate or the ratio between the averaged radial to axial velocities at the inlet.

In Xia et al.'s study, the fuel-air mixture entered the combustor via an annulus with no central jet and the inlet was oblique to the axis of the chamber. A three-dimensional flow simulation was carried out for isothermal, turbulent flow in the burner of a gas turbine. The outlet velocity profiles thus obtained were used to specify the inlet velocity conditions of the combustion chamber axisymmetrical model. The influence of the inlet and outlet boundary conditions on the flow characteristics in the chamber was assessed. Detailed calculations revealed an internal recirculation zone (IRZ) and an external recirculation zone (ERZ) in the chamber. Provided the averages of the inlet axial, radial and tangential velocity components were preserved, the shape of the applied inlet velocity distributions had a nonnegligible influence on the flow. The same overall flow pattern was realized and the lengths of the IRZ as well as the lengths of the ERZ, were nearly identical. Some small variations in the local velocity values, however, could be discerned, especially near the inlet region. This might have a significant influence on the combustion process.

The outlet boundary conditions had an obvious effect on the swirling flow near the outlet, but nearly no influence further upstream, i.e., at distances greater than about 1.3 internal diameters from the outlet for the cases considered. It was suggested that the numerical outlet boundary should be extended by about 2.0 internal diameters to eliminate this effect in the region investigated.

The authors pointed out that the choice of turbulence model has a strong effect on turbulent swirling flows, but opted for the standard k-ε turbulence model for their work.

In 1986 the k-ε and other turbulence models were evaluated by Sloan et al. with respect to their applicability in swirling flows. In 2004, Mondal et al. studied numerically the effects of the side wall expansion angle and of the type of swirler: with straight or helicoidal vanes. The swirl number was varied in the range 0.4-2.0 by varying the vane angle. Attention was focused on the central recirculation zone to qualify its size, location and strength. They reviewed the recent applications of the k-ε turbulence model in swirling flow prediction and showed that the polemic about its applicability still remains.

Many numerical results of the application of different turbulence models are currently available, and many conflicting opinions have been expressed. In 1999, Brewster et al. observed that the k-ε turbulence model was in many cases adequate for

modeling gas turbine combustors and that the need for an improved turbulence model was secondary to the need for more detailed chemical kinetics with improved modeling of the chemical/turbulence interaction. Reacting flows, involving heat transfer, mass transfer and chemical reaction in addition to fluid flow, are so complex that the deficiencies of the standard k-ε model are overlooked compared to its advantages, like simplicity and savings.

Other authors reported that the standard k-ε model had certain limitations in predicting swirling flows and proposed ad-hoc corrections. An alternative proposition to the problem was the use of a higher order turbulence model, such as the algebraic stress model or the Reynolds stress model, but these increase the computational complexity and time requirement. Thus, despite the advances in modeling turbulent flow, the standard k-ε model remained a commonly used model in the prediction of turbulent flows in combustors, as can be observed in the work of Dong and Lilley in 1994, Xia et al. in 1997, Foster et al. in 2000 and Mondal et al. in 2004.

The aerodynamics of a movable block-MB-burner, developed by the International Flame Research Foundation - IFRF (Wu and Fricker, 1971) was numerically investigated by Fudihara et al. in 2003. Five numerical grids, corresponding to five positions of the movable blocks were developed. The duct used for fuel injection, was assumed to be externally closed. The k-ε turbulence model was compared with the RNG k-ε model and the upwind differencing interpolation scheme was compared with the higher-order upwind differencing scheme using the CFX-4 simulator (Guidelines of CFX-4. 2001). The reasons for the frequently weak corroboration found between prediction and experiments on swirling flows were discussed with regard to (i) the simplifications introduced into the mathematical model, such as assuming two-dimensional flow and/or isotropic turbulence; (ii) the characteristics of the numerical techniques, such as the order of the adopted interpolation scheme or the grid boundary conditions, and (iii) the physical phenomena themselves, such as the multistability of the flow in the phenomenon of bifurcation or the vortex breakdown patterns.

The predicted swirl numbers for the two air mass flow rates tested, 1300 kg/h and 2000 kg/h, were practically identical, as observed in the experiments. A severe swirl reduction was observed along the axial direction in the annular section. With the maximum tangential aperture, an intense reverse flow was observed in the center of the quarl, also extending back into the annular section. With an intermediary tangential aperture, only the RNG k-ε model had this behavior, while with the k-ε model, reverse flow was observed only in the quarl and was insignificant in the annular section. With a null tangential aperture, no reverse flow was observed and high flow instabilities appeared.

The swirl numbers predicted by the MB burner simulation, using the RNG k-ε turbulence model and the higher-order upwind differencing interpolation scheme, were about half the experimental values obtained by Beér and Chigier, 1974, for the five ξ/ξ_m tested and were lower than an approximate analytical correlation developed by these authors for burners that use flow channeling by guidance blades or movable blocks to generate swirl.

The same happened with another channeling type of burner, the axial and tangential air entries swirl burner, whose experimental swirling numbers were also lower than the swirl numbers found in the experiments with the MB burner and than the predicted swirl numbers, as shown in Figure 1.

In 2000, Widmann et al. studied still another different type of swirl burner, a vane-cascade swirl burner, and by CFD simulation, also obtained swirl numbers well below those found by Beér and Chigier's approximate analytical correlation, which they compared with their own experiments. They concluded that the simplifications embedded in the correlation were inadequate. In addition, the authors compared the k-ε and the RNG k-ε turbulence models and found better agreement of the latter with the corresponding experimental data (Xia et al., 1997).

In the present study, the aerodynamics of the Delft-IFRF vertical furnace was computationally investigated by applying the finite volume method by means of the CFX-4 simulator and adopting the RNG k-ε turbulence model, due to its greater reliability as discussed below, and its capacity to predict a reverse flow for an intermediary swirl, not only in the quarl, as with the k-ε model, but also in the burner annular section (Fudihara et al., 2003). The aerodynamics of the furnace was obtained avoiding the intermediary determination of the burner/quarl outlet velocity profiles to serve as the inlet velocity profiles in the combustion chamber.

Three computational grids were developed for the furnace, representing three apertures of the movable block burner, as represented in Figure 2.

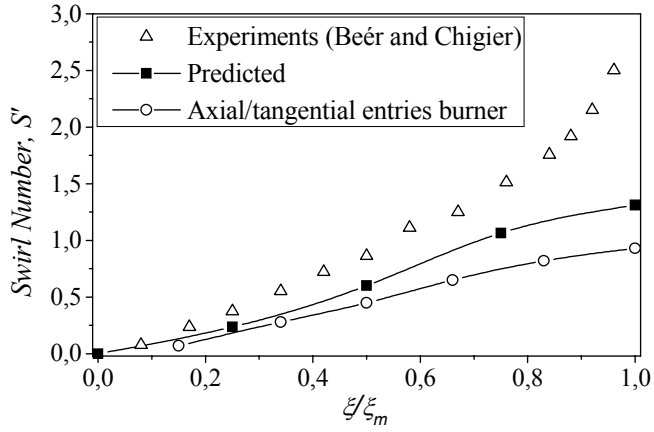

Figure 1: Movable Blocks Burner Swirl - Experiment vs Predicted.

ξ/ξ_m=0.5 ξ/ξ_m =0.75 ξ/ξ_m =1.0

Figure 2: Movable Blocks Burner - Aperture fractions = 0.5, 0.75 and 1.0.

THE FURNACE

The schematic layout shown in Figure 3 corresponds to the arrangement of a vertical furnace built at Delft University, which was tested in cooperation with the Ijmuiden Station at the IFRF (Wu and Fricker, 1971). The first 2 meters of total length of 5 m were represented on the grid. In these experiments a set of quarl configurations were tested. Both an isothermal and a fired investigation of the furnace were performed.

The MB burner, shown in Figure 4, produces swirling flow by channeling the flow. In an MB burner, combustion air enters perpendicularly to the axis through a set of tangential and normal openings, which correspond to the gaps between succeeding movable and fixed blocks. The fuel is injected into the combustion chamber through the burner inner tube.

With this burner the flow swirl can be uniformly increased or reduced by rotating the set of movable blocks in order to expand or contract the tangential openings and simultaneously contract or expand the normal openings, which respectively direct the air flow tangentially or normally at the burner entrance.

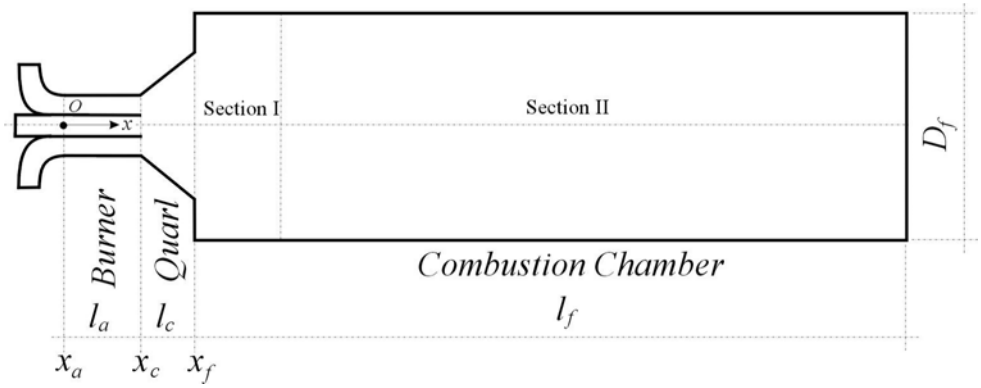

Figure 3: Schematic Layout of a Gas Furnace.

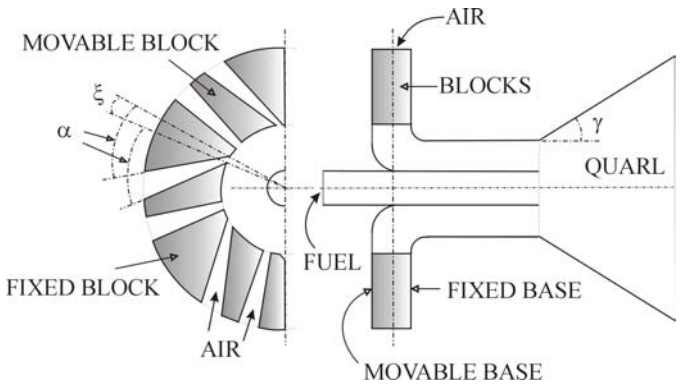

Figure 4: Schematic Layout of the Burner.

The tangential openings are characterized by the angle ξ, which varies from zero to a maximum of ξ_m. The angle between the surfaces of the openings, α, is 50° for the oblique opening surfaces. The corresponding angle for the normal opening surfaces is 0°.

Burner performance depends on the number of blocks and their geometry and size; the annular section ratio between the internal and the external radius; the ratio between the length and the width; and the quarl enlargement factor, defined by the angle γ.

The burner in this study was the same as that analyzed by Fudihara et al., 2003 with eight movable blocks located in between eight fixed blocks. The quarl used corresponded to Nozzle 2 of the experiments performed in the Delft furnace, with a quarl half expansion angle, γ, of 35°. The numerical tests were isothermal, as no fuel was supplied. Correspondingly, the burner fuel feeding pipe was closed in the grid.

The parameter l, given in Table 1, represents length, as shown in Figure 3 and the subscripts a, c and f refer to the burner, the quarl and the combustion chamber, respectively. D_f is the diameter of the combustion chamber. The origin O and the x axis of the coordinate system adopted are plotted.

Table 1: Furnace Dimensions

Parameters	Values
l_a [mm]	160
l_c [mm]	190
l_f [mm]	2000
D_f [mm]	900
α [°]	0 and 50
γ [°]	35
ξ_m [°]	12

The combustion chamber was separated into sections I and II to allow a more comprehensive examination of the profiles of the variables in Section I, where higher velocity and pressure gradients were than those observed in Section II.

MODELING

Governing Equations

A direct numerical solution of the continuity and the momentum equations is not practical for a turbulent flow because the grid would require an impractical refinement in order to represent all aspects of the eddies. Great effort has been dispensed to obtain approximate solutions for an extensive variety of types of flow. Reynolds decomposition and time averaging was the first procedure used in the development of various models of turbulent flow, which applied to the transport equations, resulted in the following equations:

Continuity Time-averaged Equation

$$\frac{\partial \rho}{\partial t} + \nabla \cdot (\rho \mathbf{v}) = 0 \qquad (1)$$

Momentum Time- averaged Equation

$$\frac{\partial \rho \mathbf{v}}{\partial t} + \nabla \cdot (\rho \mathbf{v}\mathbf{v}) = -\nabla P + \nabla \cdot \left(\upsilon - \rho \overline{\mathbf{v}'\mathbf{v}'} \right) + B \tag{2}$$

where

$$\upsilon = \left(\varphi - \frac{2}{3}\mu \right) \nabla \cdot \mathbf{v}\delta + \mu \left(\nabla \mathbf{v} + (\nabla \mathbf{v})^T \right) \tag{3}$$

The time averages are implicit for all primitive variables in these equations. The Reynolds stress $-\rho \overline{\mathbf{v}'\mathbf{v}'}$ is not null and must be calculated. The eddy viscosity hypothesis was used to derive various turbulence models. According to this hypothesis, the Reynolds stress was modeled by

$$-\rho \overline{\mathbf{v}'\mathbf{v}'} = -\frac{2}{3}\rho k\delta - \frac{2}{3}\mu_T \nabla \cdot \mathbf{v}\delta + \mu_T \left(\nabla \mathbf{v} + (\nabla \mathbf{v})^T \right) \tag{4}$$

Substituting it into Equation 2, the momentum equation became

$$\begin{aligned} &\frac{\partial \rho \mathbf{v}}{\partial t} + \nabla \cdot (\rho \mathbf{v}\mathbf{v}) = \\ &= -\nabla P' + \nabla \cdot \left(\mu_{ef} \left(\nabla \mathbf{v} + (\nabla \mathbf{v})^T \right) \right) + B \end{aligned} \tag{5}$$

where P'was defined as

$$P' = P + \frac{2}{3}\rho k + \left(\frac{2}{3}\mu_{ef} - \varphi \right) \nabla \cdot \mathbf{v} \tag{6}$$

and the effective viscosity, as

$$\mu_{ef} = \mu_T + \mu \tag{7}$$

Turbulent viscosity, μ_T, was calculated in accordance with the initial proposal of Kolmogorov and Prandtl:

$$\mu_T = C_\mu \rho \frac{k^2}{\varepsilon} \tag{8}$$

where C_μ is a constant, and the kinetic turbulent energy, k, and its dissipation rate, ε, were determined as detailed, for example, in Lixing, 1993 and in Garde, 1994.

The flow was assumed to be incompressible and isothermal.

Turbulence Model

The k-ε turbulence model has been one of the models most commonly used in engineering practice, as previously mentioned, but its poor performance for various types of flows has been widely discussed. Two differential equations, one for k and one for ε, should be solved to obtain the turbulent viscosity μ_T field. Advancement of the study of the renormalization group theory (RNG) by Yakhot and Orszag in 1986, and rectified by Yakhot and Smith in 1992, was applied to the standard k-ε model. The result was the RNG k-ε turbulence model, which allows obtaining the k-ε model constants analytically. In 1998, Morvan et al. analyzed the new model and listed its advantages in describing the flows with high or low Reynolds numbers and swirling or circulation flows, as in the present work.

The k and ε domains were obtained from the following equations:

$$\frac{\partial \rho k}{\partial t} + \nabla \cdot (\rho \mathbf{v} k) - \nabla \cdot \left(\left(\mu + \frac{\mu_T}{\nu_{kRNG}} \right) \nabla k \right) = \Pi - \rho\varepsilon \tag{9}$$

and

$$\begin{aligned} &\frac{\partial \rho \varepsilon}{\partial t} + \nabla \cdot (\rho \mathbf{v} \varepsilon) - \nabla \cdot \left(\left(\mu + \frac{\mu_T}{\nu_{\varepsilon RNG}} \right) \nabla \varepsilon \right) = \\ &= \left(C_{1RNG} - C_\eta \right) \frac{\varepsilon}{k} \Pi - C_{2RNG} \rho \frac{\varepsilon^2}{k} \end{aligned} \tag{10}$$

where

$$\Pi = \Pi_S - \frac{2}{3} \nabla \cdot \mathbf{v} \left(\mu_{ef} \nabla \cdot \mathbf{v} + \rho k \right) \tag{11}$$

$$\Pi_S = \mu_{ef} \nabla \mathbf{v} \cdot \left(\nabla \mathbf{v} + (\nabla \mathbf{v})^T \right) \tag{12}$$

$$C_\eta = \frac{\eta \left(1 - \frac{\eta}{\eta_0} \right)}{1 + \beta_{RNG} \eta^3} \tag{13}$$

$$\eta = \left(\frac{\Pi_S}{\mu_T} \right)^{0.5} \frac{k}{\varepsilon} \quad (14)$$

where ν is the turbulent Prandtl number and C_{1RNG}, C_{2RNG}, ν_{kRNG}, $\nu_{\varepsilon RNG}$, β_{RNG} and η_0 are the model constants.

Swirl Number

The swirl number S is a dimensionless parameter that characterizes the swirl intensity of the flow in a section. It is defined as

$$S = \frac{G_w}{G_u r_i} \quad (15)$$

where G_w is the axial flux of the gas angular momentum, G_u is the axial flux of the axial momentum and r_i is a characteristic length.

The axial fluxes of the angular and of the axial gas momentum can be obtained with the equations

$$G_w = 2\pi \int_0^{r_i} (wr)\rho u r \, dr \quad (16)$$

and

$$G_u = 2\pi \int_0^{r_i} u\rho u r \, dr + 2\pi \int_0^{r_i} P r \, dr \quad (17)$$

which are functions of the tangential velocity, w, of the axial velocity, u, and of the static pressure, P.

A modified swirl number S' is defined by removing the term containing the static pressure from G_u, as in Fudihara et al.,2003 and in Widmann et al.,2000, who observed that S' was very different from S.

The upper limit of the integrals of G_w and G_u is r_i, the characteristic length, equal to half the diameter of the external pipe in the burner annular section and to half the diameter in the combustion chamber. It varied axially along the quarl due to the expansion of the conical wall.

An abrupt expansion is observed when the flow leaves the quarl and enters the combustion chamber. Despite the unique velocity profile, two different swirl numbers can be defined at the edge between these two parts, due to the existence of two characteristic lengths at this position: on the quarl side, r_i is half the diameter of the quarl exit, while on the combustion chamber side, r_i is half the diameter of the combustion chamber. These two swirl numbers are correlated, with their ratio corresponding to the inverse of the ratio of the respective characteristic lengths.

Boundary Conditions

The numerical conditions prescribed for the boundaries are fundamental in obtaining a solution closer to that in the experimental data. This was corroborated by Dong and Lilley in 1994 and by Xia et al. in 1997, who applied CFD to investigate the effect of boundary conditions on swirling flows.

Xia et al., 1997, compared the effects of two outlet boundary conditions, namely mass flow rate and uniform pressure, as defined by the CFDS-FLOW3D simulator (Guidelines of CFX-4, 2000). They observed a slight divergence between the predicted velocity distributions in about 40% of the chamber, upstream from the outlet boundary. They recognized these variances as due to a radial pressure gradient ensuing from the mass flow rate boundary condition, in contrast to the condition of uniform pressure. In both cases the flow in the chamber was arranged to provide a constant normal velocity gradient at the outlet boundary. The uniform pressure boundary condition was recommended for at the outlet boundary when the fluid vented to a large volume, such as when it was discharged into the atmosphere. However, if a highly uneven velocity gradient persisted near the outlet boundary, as a consequence of an irregular geometry, for example, the pressure profile at the boundary would be nonuniform, even if the fluid was discharged into an unconfined environment. In addition, these uneven flow and pressure fields could extend for a considerable length in the environment.

The usual boundary conditions considered in the simulation to reproduce an experiment are (i) uniform pressure profile, (ii) velocity profile or (iii) mass flow rate, which can be prescribed at the inlet or at the outlet boundary of a grid.

Boundary conditions in transient flow simulations are particularly difficult to establish, since the flow at the boundary can also change with time. It is usual to ignore this time dependency and adopt invariant parameters at the boundary, such as those of a steady state flow, although this procedure can compromise the consistency of transient predictions.

a) Boundary Condition at the Inlets

At the burner air inlets, the uniform pressure boundary condition was prescribed. The parameters k_{in} and ε_{in} were estimated from

$$k_{in} = 0.002\mathbf{v}_{in}^2 \quad (18)$$

and

$$\varepsilon_{in} = k_{in}^{1.5} / 0.3d_h \quad (19)$$

as proposed by Khalil et al. in 1975, where $\mathbf{v}_{in}$ is the inlet velocity and d_h is the inlet hydraulic diameter.

The effective turbulent viscosity, defined in Equation (7), was computed at the inlet boundary by extrapolation from the downstream value because k and ε usually vary rapidly near this boundary, causing large numerical errors when the viscosity gradients are calculated.

The fuel feeding duct was assumed to be closed by a wall boundary condition.

b) Boundary Condition at the Outlet

The mass flow rate boundary condition was prescribed at the chamber outlet. In so doing, the pressure, k and ε were extrapolated from the upstream value.

c) Boundary Conditions at the Walls

The burner annular region, around the fuel feeding duct, was numerically delineated by implementing the thin surface boundary condition. The wall boundary condition was set at the remainder of the external surfaces of the grid. The movable and fixed blocks of the burner were not represented, but the openings between them were.

A stagnant condition exists at the wall surface, so the wall-function method was applied for the layer close to the walls, in accordance with Launder and Spalding's proposal in 1974.

Complementary boundary conditions were automatically prescribed by the CFX-4 simulator (Guidelines of CFX-4, 2000). Since the uniform pressure boundary condition was prescribed at the burner inlets and the mass flow rate boundary condition at the chamber outlet, the Neumann boundary condition for the velocity field was automatically implemented at these boundaries.

NUMERICAL COMPUTATION

Numerical Method

The continuity and momentum time-averaged equations were numerically solved by the finite volume method in structured and nonstaggered grids for the variables by means of the computational simulator CFX, version 4.4 .

The geometry of the grid was constructed using the multiblock method. The irregular blocks and the equations in the Cartesian coordinate system were transformed into regular blocks and solved in a generalized coordinate system.

The pressure velocity coupling was realized by the SIMPLEC algorithm.

The numerical interpolations for the advection terms were initially carried out by the first-order upwind differencing scheme and then by the second-order higher-order upwind differencing scheme.

The steady-state solution was obtained using the pseudo time-step method, where the time step varied between 0.0001 and 0.01 seconds, arbitrarily chosen, according to the convergence performance. Additional details can be found in Patankar, 1980 and Maliska, 1995.

Grid System

Three computational grids, corresponding to three burner aperture angles: ξ/ξ_m equal to 1.0, 0.75 and 0.5 were developed for the furnace. Nearly 119,000 control volumes were employed in the grid for ξ/ξ_m = 1.0 and 217,000 in the grids for ξ/ξ_m = 0.75 and 0.5.

The same air mass flow rate as that used in the isothermal tests for the Delft University's furnace (Wu and Fricker, 1971), 1320 kg/h, was supplied to the burner for the three aperture angles. For ξ/ξ_m = 1.0, the air entered the burner only through its tangential openings, while for ξ/ξ_m = 0.75 and 0.5, the air entered partly through the normal and partly through the tangential openings.

Solution Strategy and Convergence Criterion

The air in the furnace was stagnated at the beginning of the simulation. With application of the boundary conditions and calculation, a reverse flow was abruptly formed as then ascertained by successive instantaneous flow visualizations. This phenomenon, characteristic of a vortex breakdown, disturbed severely the stability of the numerical convergence.

The convergence performance of the first-order upwind differencing interpolation scheme for the numerical interpolation was better than that of the second-order higher-order upwind differencing, probably due to its inadequate higher dissipation of velocity gradients.

The upwind differencing scheme was applied from the startup until formation of the reverse flow, when the simulation was temporarily stopped. Next, upwind differencing was substituted by higher-order upwind differencing and the simulation was restarted. The initial condition of the new startup was the last predicted velocity, pressure, k and ε fields, with the reverse flow already formed.

After disturbing the steady state-flow, the flow would return to the original pattern when the source of the disturbance was removed. The swirler apparatus could strongly disturb the structure of a reverse vortex core, as pointed out by Lucca-Negro and O'Doherty in 2001. It can be assumed that the results of the first simulation with upwind differencing corresponded to a disturbed flow. Changing to higher-order upwind differencing, as the simulation advanced, the disturbance dissipated and the flow returned to the steady-state condition.

This approach was successfully applied for ξ/ξ_m = 1.0 and 0.75. For ξ/ξ_m = 0.5, after the reversion of flow and the change in interpolation scheme to the higher-order upwind differencing scheme, the calculations invariably diverged after some iteration.

A transient simulation was performed for ξ/ξ_m = 0.5, using as the initial condition the same previously calculated profiles, the upwind differencing scheme and the fully implicit backward Euler differencing with a first-order time-stepping method. Although the transient simulation could not run off the numerical divergence, an unstable flow was observed in the 2.5 seconds of flow inspection, mainly in the combustion chamber. The time step was 0.01 seconds. One possible explanation for the numerical divergence found is that it was due to the physical phenomenon itself, as a consequence of the lower swirl intensity resulting from the smaller aperture of the tangential openings in the burner. This could cause an unstable or even a multistable flow with intermittent relocations involving two or more distinct stable flows, as described by Sarpkaya in 1971 and Faler and Leibovich in 1977. The iterative calculation was not able to manage these fast flow instabilities.

The corroboration of the results with the experiments is a direct process when there is only one steady-state pattern for a given operational condition. In this case the predicted and experimental patterns would be the same, independent of the path or strategy adopted to reach the steady state, according to the procedure described previously.

On the other hand, Sarpkaya, 1971 and Faler and Leibovich, 1977, obtained experimentally diverse patterns of flow reversal in swirling flows for the same operational condition, using water as fluid. In the case of multiple steady-state patterns, the predicted and the experimental patterns should be equivalent.

RESULTS AND DISCUSSION

Profiles of Flow Velocity in the Combustion Chamber

The combustion chamber was divided into two sections, as indicated in Figure 1. The length of Section I was 250 mm and the length of Section II was 1750 mm, for a total length l_f = 2000 mm. In Section I, the flow parameters were displayed along the diameter of six chamber cross sections, spaced 50 mm apart. In Section II, the profiles were displayed in eight cross-sections, 250 mm apart, including once more the cross section at the boundary with Section I. At $x\text{-}x_f$ = 0, the flow velocity profile is the profile of the fluid leaving the burner/quarl.

a) Mean Axial Velocity Profiles

Profiles of the axial velocity, $\mathbf{v}_x$, are shown in Figures 5 and 6 for ξ/ξ_m = 1.0 and 0.75, respectively. The air left the quarl and entered the combustion chamber as a high velocity jet, displaced from the longitudinal axis due to its centrifugal force. A reverse flow, formed inside the combustion chamber, moved back into the quarl, as can be seen at the inlet of Section I for both aperture angles. As expected, the reverse flow became more intense with the swirl, which was controlled by increasing the aperture of the tangential openings of the burner.

b) Mean Tangential Velocity Profiles

Profiles of the tangential velocity, $\mathbf{v}_t$, are shown in Figures 7 and 8 for ξ/ξ_m= 1.0 and 0.75, respectively. The flow maintained a rotating movement along the extent of the chamber. The direct and reverse flows rotated almost as a single body, and it was not possible to distinguish the limit between these flows by examining only the tangential velocity component, mainly farther downstream. The more intense reverse flow found for ξ/ξ_m = 1.0, as mentioned above, was due to the higher tangential velocities.

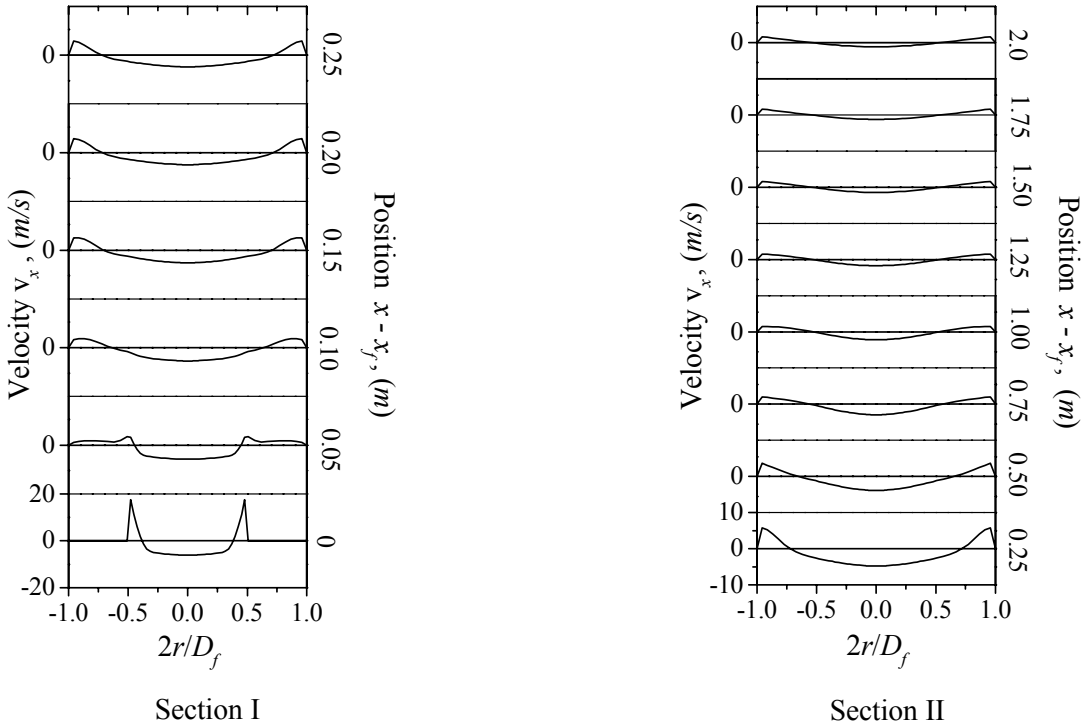

Figure 5: Mean Axial Velocity - $\xi/\xi_m = 1.0$.

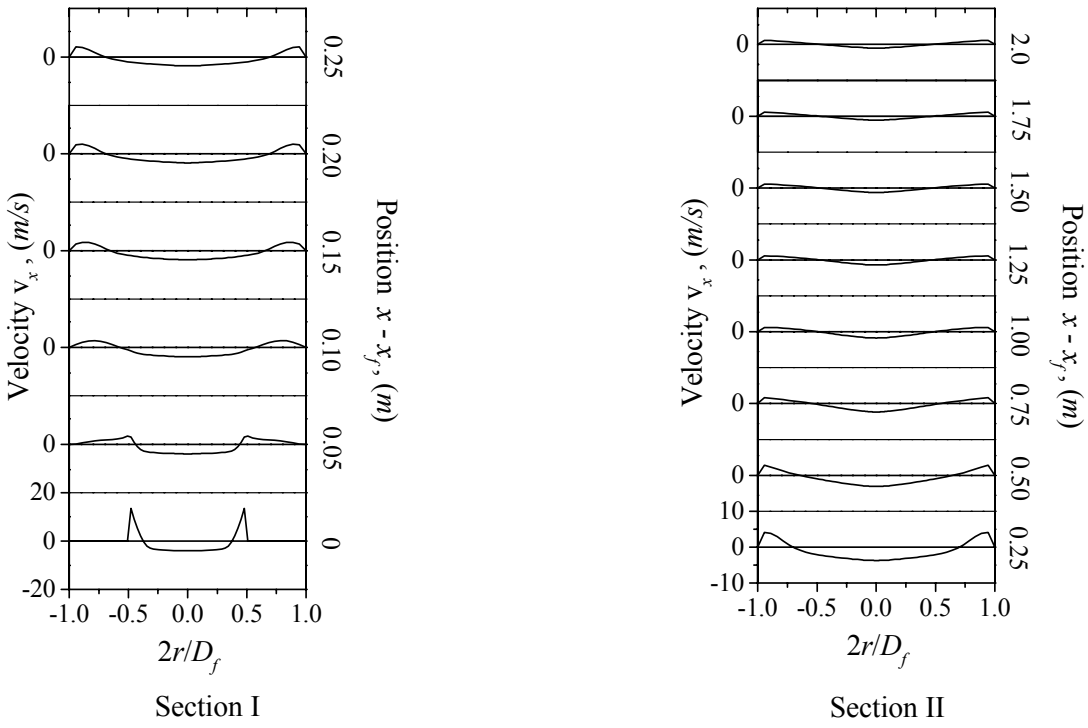

Figure 6: Mean Axial Velocity - $\xi/\xi_m = 0.75$.

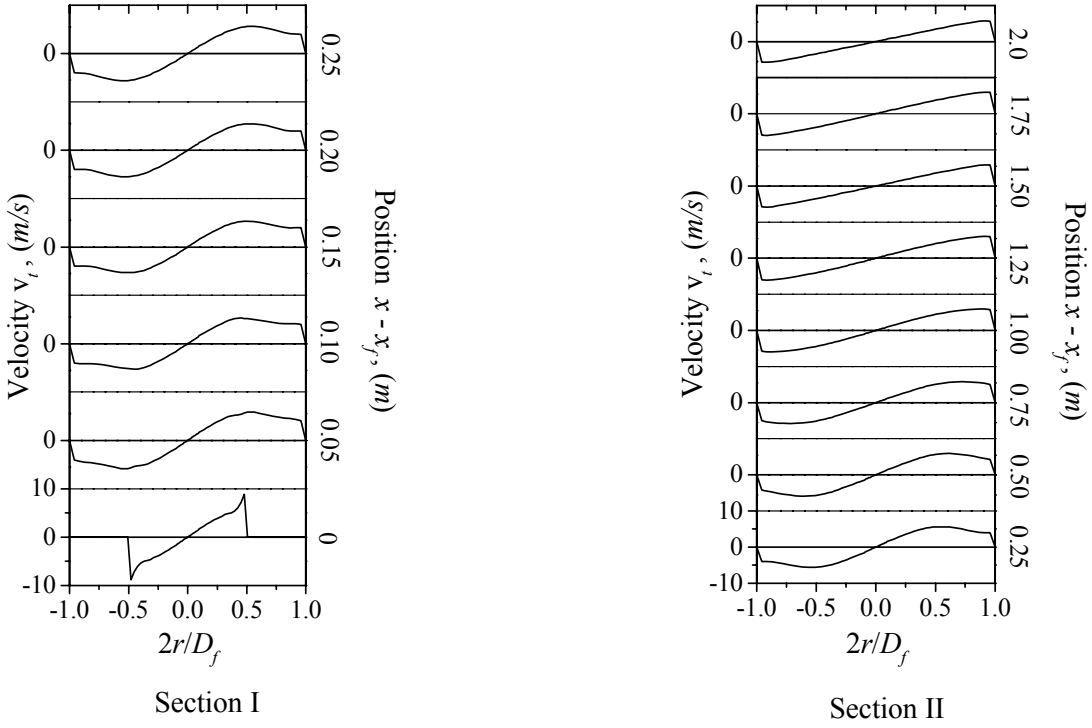

Figure 7: Mean Tangential Velocity - $\xi/\xi_m = 1.0$.

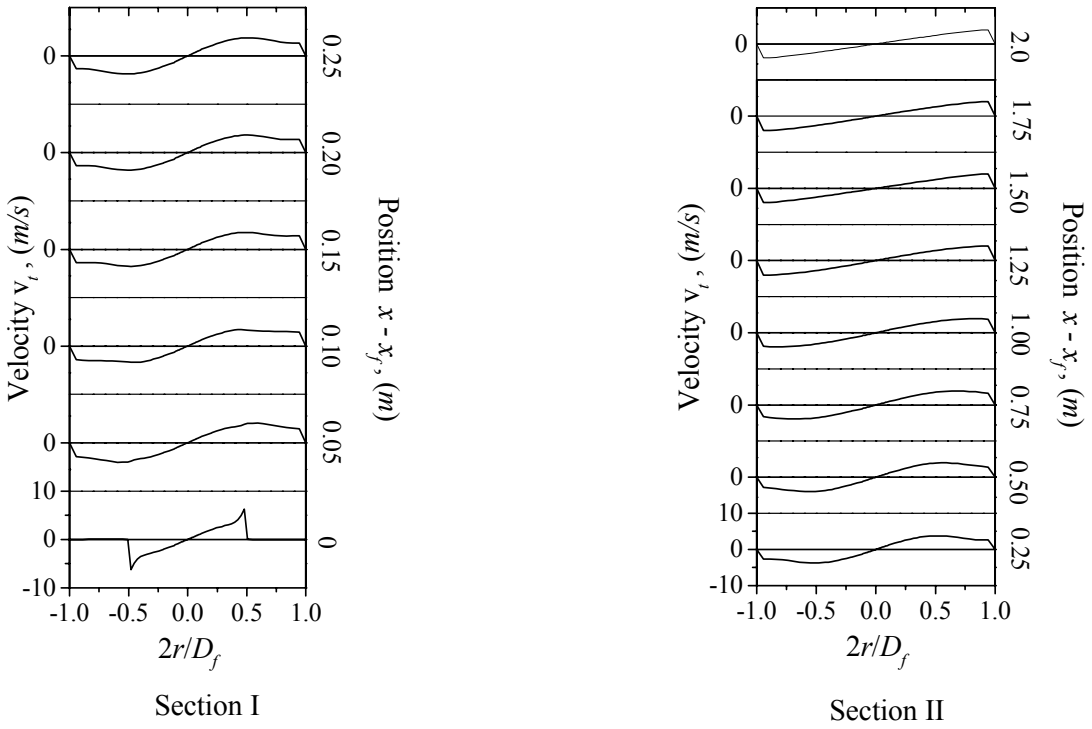

Figure 8: Mean Tangential Velocity - $\xi/\xi_m = 0.75$.

Near the exit of the quarl, the jet pattern in the chamber was similar to a type B flow, as classified by Beér and Chigier, 1974, with an air jet surrounding a region of reverse flow. Farther downstream, the flow pattern became similar to a type C flow, where a reverse flow persisted in the center of the chamber, still enclosed by the direct flow closer to the wall.

As the fluid traversed the quarl expansion and entered the combustion chamber of the higher cross-section area, its axial velocity was reduced. A countercurrent stream was produced by the swirling flow and shared the chamber cross-section area with the direct flow. The net air mass flow rate in each cross section is the difference between the direct and the reverse flow rates. Increasing the swirl, the counter stream became more intense, and consequently the direct mass flow also increased.

At the combustion chamber outlet, $x\text{-}x_f = 2.0$ m, a reverse flow was created by an air stream coming from outside the chamber grid, such that, part of the outlet boundary acted as an inlet boundary. The net air flow rate through the chamber outlet was equal to the air flow rate supplied to the burner inlets.

At the axial position, $x\text{-}x_f = 0.25$ m, the reverse air mass flow was intense. For $\xi/\xi_m = 1.0$, it was about 2.6 times larger than the air mass flow rate supplied to the burner. For $\xi/\xi_m = 0.75$, the reverse flow was about twice as large. Farther downstream, a reduction in the reverse flow was accompanied by a reduction in the direct flow.

Figures 5 to 8 show the predicted velocity profiles at the chamber outlet, where the Neumann boundary condition was implemented by the simulator. These and the predicted profiles of pressure, k or ε, which were calculated from extrapolation of the upstream conditions, were not uniform at the chamber outlet.

c) Mean Radial Velocity Profiles

Profiles of the radial velocity component in Section I are shown in Figure 9 for $\xi/\xi_m = 1.0$ and 0.75. This velocity component was not null at the chamber inlet and was rapidly dissipated still in Section I, as shown.

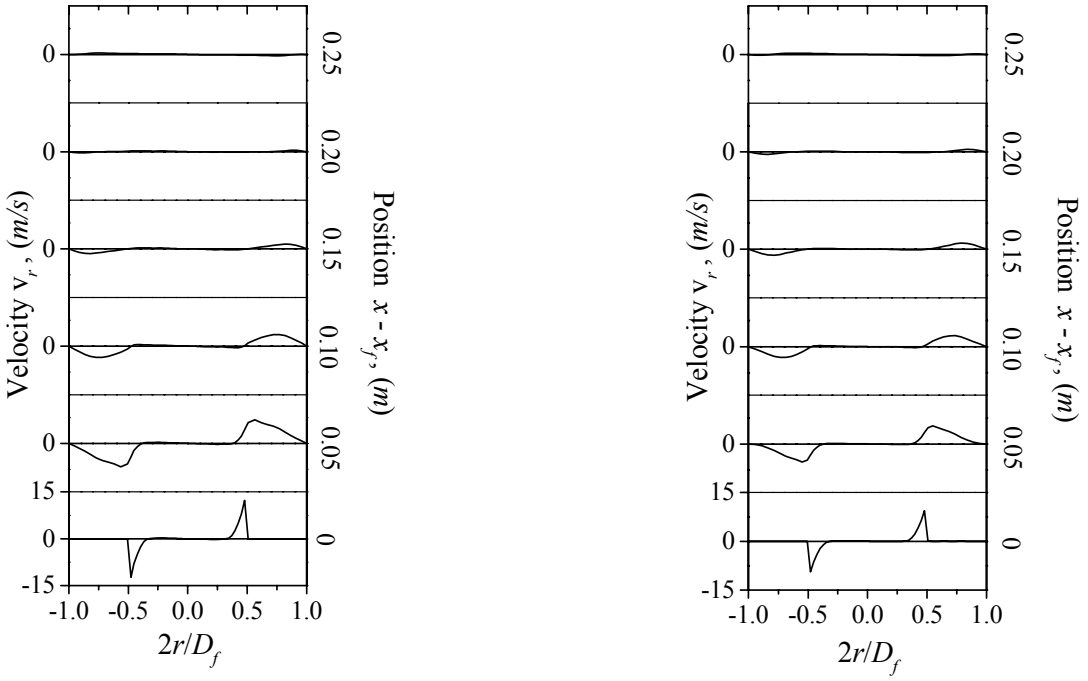

Figure 9: Profiles of Mean Radial Velocity along Section I.

The simplified boundary conditions usually assumed at the inlet of a combustion chamber, in the absence of more realistic information that reproduces the complex flow which exists at the burner exit, have the advantage of economizing on computer requirements, which allows the use of more refined grids. Their adoption, nonetheless, can generate unreliable results and is an inappropriate practice.

In 1986, Sloan et al. observed that in swirling flows the radial velocity component affects the extension of the circulation region. Xia et al., 1997, proposed a complementary parameter, the radial number, obtained in the same way as the swirl number, but using for its estimation the radial distribution of the radial velocity in place of the tangential velocity.

In Figure 10 the distribution of the axial velocity component in the furnace is presented, for $\xi/\xi_m = 1.0$ and 0.75, obtained in this work for the Delft-IFRF furnace. The reverse flow occupying the central part of the cylindrical chamber along the longitudinal axis originated in an air stream returning from outside the grid domain through the combustion chamber outlet boundary. The reverse flow expanded slowly and then accelerated. Near the inlet of the combustion chamber it shrank and entered the burner along the external surface of the fuel feeding duct wall.

The reverse flow was more intense for $\xi/\xi_m = 1.0$ than for $\xi/\xi_m = 0.75$, but the volume of the combustion chamber occupied by the reverse flow was only slightly larger for the first aperture, as can be observed by comparing Figures 10 (a) and 10(b). The existence of a back flow from the combustion chamber into the burner suggests that, during operation, the burner may need protection from the hot combustion gases.

In Figure 10 the experimental plot presented by Wu and Fricker, 1971, is also shown by dashed lines superposed on the map for $\xi/\xi_m = 1.0$. This plot represents the flow contours for the highest swirl number presented by these authors. When compared with the predicted contours, their experiments showed a thinner reverse flow and a less intense spread of the air jet at the entrance of the combustion chamber.

Further, no corner circulation region or ERZ was predicted by the simulation in the combustion chamber, as suggested by the two perpendicular dashed lines close to the circular wall of the combustion chamber.

In 1995, Kenbar et al. realized flow measurements in a semi-industrial-scale natural-gas-fired furnace and obtained distributions of time-averaged axial, tangential and radial velocity components for two swirl intensities along the furnace. They observed practically no ERZ or at most a quasi-static condition, which was attributed to the large furnace-to-quarl exit diameter ratio of 5.0. The corresponding ratio for the present furnace was about 2.0.

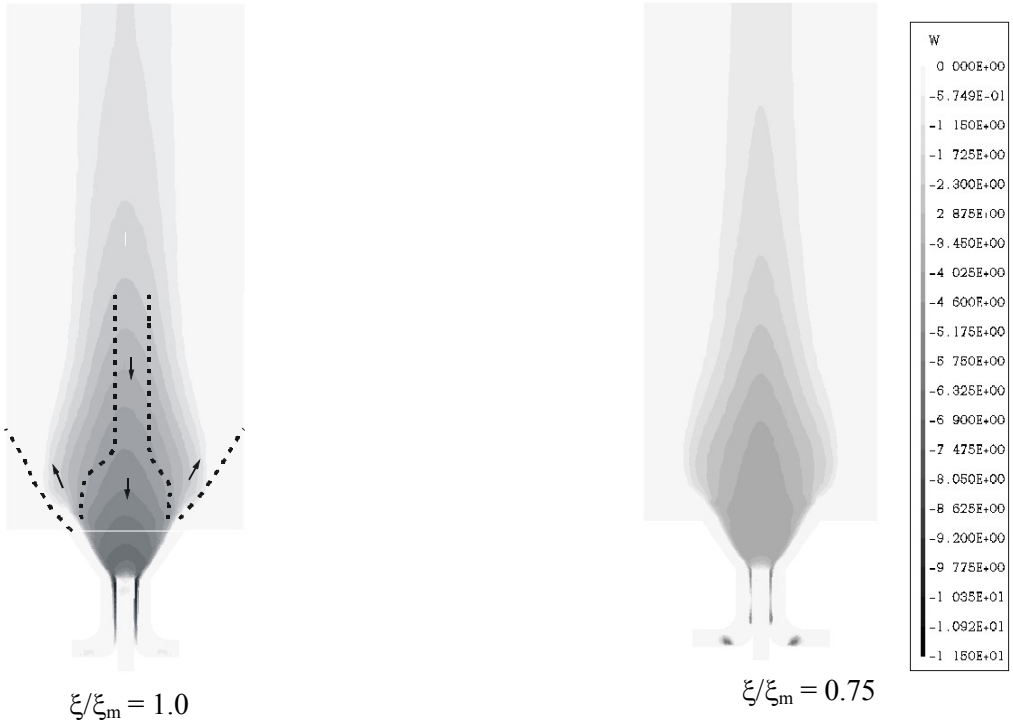

$\xi/\xi_m = 1.0$ $\xi/\xi_m = 0.75$

Figure 10: Maps of Mean Axial Velocity – Present work.
Wu and Fricker - Dashed lines.

Swirl Number

In Figure 11 the swirl number variation along the furnace is presented for $\xi/\xi_m = 1.0$ and 0.75, where l_k indicates the length of the burner, quarl or combustion chamber and x_k is equal to the axial positions x_a, x_c and x_f, as shown in Fig. 1.

The swirl number S' decreased along the annular duct in the burner and along the quarl, as expected and as observed in the experiments by Edwards et al. in 1993, Li and Tomita in 1994, and Parchen and Steenbergen in 1998, for swirling flows in pipes.

For $\xi/\xi_m = 1.0$, the decay was about 40% in the annular duct and 74% in the quarl. For $\xi/\xi_m = 0.75$, the decays of S' in the annular duct and in the quarl were approximately 20% and 67%, respectively.

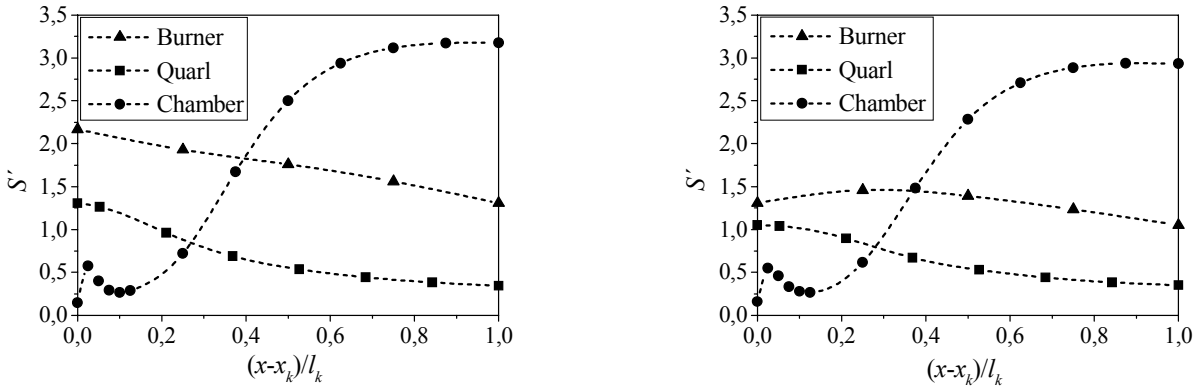

$\xi/\xi_m = 1.0$ $\xi/\xi_m = 0.75$

Figure 11: Swirl Number Profiles.

At the inlet of the combustion chamber, S' increased and then decreased slightly, reaching a minimum; it then increased sharply along the subsequent 60% of the chamber length, stabilizing in the remaining part. This behavior was similar for both aperture angles. The increase in S' between the inlet and the outlet of the combustion chamber was about 2100% for $\xi/\xi_m = 1.0$ and about 1700% for $\xi/\xi_m = 0.75$. Considering that S' varies inversely with the characteristic length, as defined in Eq.15, the significant increase in S' that occurred in the combustion chamber appeared more unusual, since the characteristic length of the chamber was larger than characteristic lengths of the burner and the quarl. It was the maintenance of the tangential velocity component in the combustion chamber and the reduction of the axial velocity component that caused an increase in the ratio of the tangential to the axial velocity, which made up for and surpassed the effect of the larger characteristic length.

CONCLUSIONS

In this work the air flow in a furnace composed of a movable block swirl burner connected to a cylindrical combustion chamber by a quarl was computationally investigated. A three-dimensional study was performed by means of the finite volume method. The numerical grid was developed by the multiblock technique. The turbulence phenomenon was addressed by the RNG k-ε model.

The profiles of the mean velocity components, axial, tangential and radial, were determined for two different aperture angles of the oblique air feeding entrances of the burner.

As it left the quarl, the air entered the combustion chamber as a high-velocity jet. A reverse flow, formed inside the combustion chamber, move back into the quarl and into the burner annular section at the tested aperture angles.

The reverse flow was more intense with the increase in the swirl, resulting from the larger aperture of the tangential openings of the burner. It consisted in part of a fraction of the direct flow that was reversed and in part by external air coming from upstream of the outlet boundary; it was more intense closer to the burner.

The flow maintained a rotating movement around the longitudinal axis of the combustion chamber. The direct and reverse flows rotated almost as a single body, mainly farther downstream.

The radial velocity component had an impact on the furnace aerodynamics and can not be neglected

as a boundary condition at the combustion chamber inlet, as in some previous chamber simulations.

Estimating the axial velocity profile at the inlet boundary from the known mass flow rate may be a poor approximation.

The comparison between the map of the predicted axial velocity and the experimental map of Wu and Fricker, 1971, which delineates the limits between direct and reverse flows, showed that the predicted cross-flow area of the reverse flow as well as the predicted spread of the air jet into the combustion chamber were relatively closer − but larger − than those observed in the experiment.

The reverse flow was more intense for $\xi/\xi_m = 1.0$ than for $\xi/\xi_m = 0.75$, but the volume of the combustion chamber occupied by the reverse flow was only slightly larger for the first aperture. The existence of a back flow from the combustion chamber into the burner suggests that, in an operational furnace, the burner may need to be protected from the hot combustion gases.

The comparison of the velocity distribution in the burner and quarl of the furnace, obtained in the present study, with the results of Fudihara et al., 2003, for the array burner plus quarl, where the mass flow rate boundary condition was applied at the quarl exit, showed analogous results for $\xi/\xi_m = 0.75$ and 1.0. Unlike the previous study, however, no numerical convergence was found for $\xi/\xi_m = 0.5$, probably due to the very unstable flow verified in the combustion chamber, owing to the low swirl intensity.

The swirl number decayed along the burner and along the quarl, as expected. On the other hand, it rose sharply along the combustion chamber, in an unforeseen way, although the swirl number is an inverse function of the characteristic length, which is greater in the combustion chamber than in the preceding parts.

When a swirl number is associated with a flow condition, the precise axial location where it was determined should be specified, since it can change significantly along the furnace.

The aerodynamics of the furnace was obtained, thus avoiding intermediary calculation of the burner/quarl outlet velocity profiles for use as the inlet velocity profiles in the combustion chamber.

ACKNOWLEDGEMENT

The authors are grateful to FAPESP - Fundação de Amparo à Pesquisa do Estado de São Paulo - Brazil (grant number 00/14390-5), for the financial support that made this work possible.

NOMENCLATURE

k	turbulent kinetic energy,	m^2/s^2
r	radius,	m
r_i	characteristic length,	m
t	time,	s
u	axial velocity component,	m/s
w	tangential velocity component,	m/s
v	velocity vector,	m/s
B	body force,	N/m^3
G_u	axial flux of the linear momentum	(-)
G_w	axial flux of the angular momentum	(-)
P	pressure,	N/m^2
S, S'	swirl number	(-)

Constants

C_μ	0.085	(-)
C_{1RNG}	1.42	(-)
C_{2RNG}	1.68	(-)
β_{RNG}	0.015	(-)
η_0	4.38	(-)
ν_{kRNG}	0.7179	(-)
$\nu_{\varepsilon RNG}$	0.7179	(-)

Greek Letters

α	inclination angle of the block surface	(-)
β	volumetric expansion coefficient,	K^{-1}
δ	unit tensor	(-)
ε	dissipation rate of k,	m^2/s^3
γ	half angle of the quarl	(-)
φ	bulk viscosity,	kg/ms
μ	molecular viscosity,	kg/ms
ρ	density,	kg/m^3
ξ	aperture angle of the oblique inlet	(-)

REFERENCES

Beér, J. M. and Chigier, N. A., Combustion Aerodynamics, Applied Science Publis Ltd., 264p (1974).

Brewster, B. S., Cannon, S. M., Farmer, J. R. and Meng, F., Modeling of Lean Premixed Combustion in Stationary Gas Turbines, Progress

in Energy and Combustion Science, 25, 353-385 (1999).

Dong, M. and Lilley, D. G., Inlet Velocity Profile Effects on Turbulent Swirling Flow Predictions, Journal of Propulsion and Power, 10(2), 155-160 (1994.).

Edwards, R. J., Jambunathan, K., Button, B. L. and Rhine, J. M., Comparison of Two Swirl Measurement Techniques, Experimental Thermal and Fluid Science, 6(1), 5-14 (1993).

Faler, J. H. and Leibovich, S., Disrupted States of Vortex Flow and Vortex Breakdown. The Physics of Fluids, 20(9), 1385-1400 (1977).

Foster, P. J., Macinnes, J .M. and Schubnell, F., Isothermal Modelling of a Combustion System with Swirl: A Computational Study, Combustion Science and Technology, 155, 51-74 (2000).

Fudihara, T. J., Goldstein, L. and Mori, M., The Three-Dimensional Numerical Aerodynamics of a Movable Block Burner, Brazilian Journal of Chemical Engineering, 20(4), 391-401 (2003).

Garde, R. J., Turbulent Flow, John Wiley & Sons Inc, New Delhi, India, 287p (1994).

Guidelines of CFX-4, Version 4.4, AEA Technology, Harwell Laboratory, United Kingdom (2001).

Gupta, A. K., Lilley, D. G. and Syred, N., Swirl Flows. Abacus Press, England (1984).

Kenbar, A. M. A., Beltagui, S. A. and Maccallum, N. R. L., Combustion Aerodynamics of a Gas-Fired Furnace with Peripheral Fuel Injection. Experimental Thermal and Fluid Science, 10(3), 335-346 (1995).

Khalil, E. E., Spalding, D. B. and Whitelaw, J. H., The Calculation of Local Flow Properties in Two-Dimensional Furnaces, International Journal of Heat and Mass Transfer, 18, 775-791 (1975).

Launder, B. E. and Spalding, D. B., The Numerical Computation of Turbulent Flows, Computer Methods in Applied Mechanics and Engineering, 3, 269-289 (1974).

Li, H. and Tomita, Y., Characteristics of Swirling Flow in a Circular Pipe, Journal of Fluids Engineering, 116(2), 370-373 (1994).

Lilley, D.G., Swirl flows in combustion: A review, AIAA J., 15(8), 1763-1778 (1977)

Lixing, Z., Theory and Numerical Modelling of Turbulent Gas-Particle Flows and Combustion, Science Press, 231p. (1993).

Lucca-Negro, O. and O'Doherty, T., Vortex Breakdown: A Review. Progress in Energy and Combustion Science, 27, 431-481 (2001).

Maliska, C. R., Transferência de Calor e Mecânica dos Fluidos Computacional, LTC-Livros Técnicos e Científicos Editora S.A Publishing Corporation, 424p, (1995).

Mondal, S., Datta, A. and Sarkar, A., Influence of Side Wall Expansion Angle and Swirl Generator on Flow Pattern in a Model Combustor Calculated with a k–ε Model, International Journal of Thermal Sciences, 43, 901-914 (2004).

Morvan, D., Porterie, B., Larini, M. and Loraud, J. C., Numerical Simulation of Turbulent Diffusion Flame in Cross Flow, Combustion Science and Technology, 140, 93-122 (1998).

Parchen, R. R. and Steenbergen, W., Experimental and Numerical Study of Turbulent Swirling Pipe Flows, Journal of Fluids Engineering, 120(1), 54-61 (1998).

Patankar, S. V., Numerical Heat Transfer and Fluid Flow, Hemisphere Publishing Corporation, 424p, (1980).

Sarpkaya, T., On Stationary and Travelling Vortex Breakdowns. Journal of Fluid Mechanics, 45, 545-559 (1971).

Sloan, D. G., Smith, P. J. and Smoot, L. D., Modeling of Swirl in Turbulent Flow Systems, Progress in Energy and Combustion Science, 12, 163-250 (1986).

Syred, N. and Beér, J. M., Combustion in swirling flows: A review, Combustion and Flame, 23, 143–201 (1974).

Vanoverberghe, K. P., Van Den Bulck, A. E. V. and Tummers, M.J., Confined Annular Swirling Jet Combustion, Combustion Science and Technology, 175, 545-578 (2003).

Widmann, J. F., Charagundla, S. R. and Presser, C., Aerodynamic Study of a Vane-Cascade Swirl Generator, Chemical Engineering Science, 55, 5311-5320 (2000).

Wu, H. L. and Fricker, N., An Investigation of the Behavior of Swirling Jet Flames in a Narrow Cylindrical Furnace, Chapter IX. IFRF technical paper (1971).

Xia, J. L., Smith, B. L., Benim, A. C., Schmidli, J. and Yadigaroglu, G., Effect of Inlet and Outlet Boundary Conditions on Swirling Flows, Computers & Fluids, 26(8), 811-823 (1997).

Yakhot, V. and Orszag, S. A., Renormalization Group Analysis of Turbulence, Journal of Scientific Computing, 1, 3-51 (1986).

Yakhot, V. and Smith, L. M., The Renormalization Group, the ε-Expansion and Derivation of Turbulence Models, Journal of Scientific Computing, 7, 35-61 (1992).